IEEE Access
Multidisciplinary | Rapid Review | Open Access Journal

Received 8 April 2024, accepted 7 May 2024, date of publication 9 May 2024, date of current version 16 May 2024.

Digital Object Identifier 10.1109/ACCESS.2024.3399540

RESEARCH ARTICLE

Simultaneous Multi-Beam Pattern Synthesis of Subarray via Alternating Projection

ZHONGTIAN JING, YUBING HAN, (Member, IEEE), YUCHEN FENG, AND LEI XIAO
School of Electronic and Optical Engineering, Nanjing University of Science and Technology, Nanjing, Jiangsu 210094, China

Corresponding author: Yubing Han (hanyb@njust.edu.cn)

This work was supported in part by the National Natural Science Foundation of China under Grant 62371236.

ABSTRACT For a large-scale array, the subarray technology can save the radio frequency (RF) channels. However, the use of subarray technology often tends to reduce the beamforming performance of the array. In some specific scenarios, it is necessary to use simultaneous multi-beam technology for target search. Exploring methods to simultaneously achieve multi-beamforming while reducing radio frequency channels is a worthwhile research endeavor. This paper introduces an innovative application of hybrid beamforming structure to the realm of beam synthesis and proposes an algorithm for simultaneous multi-beam pattern synthesis in subarrays. This method weights the received signal of the array twice. Initially, the analog signal received by each antenna unit undergoes the first weighted, accomplished by incorporating a phase shifter after each antenna. After the initial weighted, the analog signals proceed into their respective subarray channels, where they undergo a second step of weighted after being converted into digital signals. The second step of weighted involves digital beamforming of the subarray signals, utilizing multiple sets of weights, to achieve simultaneous multibeam. The algorithm can obtain an element weighted vector and a subarray weighted matrix. Based on the alternating projection (AP) algorithm, the property of the Kronecker product, and the definition of the Khatri-Rao product, the optimal element weighted vector and subarray weighted matrix can be obtained by solving the 2-norm minimization problem.

INDEX TERMS Subarray, synthesis algorithm, multiple simultaneous patterns, alternating projection.

I. INTRODUCTION

Pattern synthesis algorithm has a very wide range of applications in the fields of radar sensors, radio astronomy and satellite communications. At present, the research of pattern synthesis algorithms is very mature. Power pattern synthesis methods such as Dolph-Chebyshev synthesis [1] and Taylor synthesis [2] can be used to obtain the desired patterns by changing the magnitude of the weights. Those methods are fast and work well on side lobe control, but they are difficult to form the complicated main lobe shapes. Stochastic optimization synthesis algorithms such as particle swarm synthesis [3] and genetic algorithm synthesis [4] have an advantage on main lobe shapes control, but needs higher requirements of the equipment. In recent years, the array response control technology proposed based on adaptive array theory has attracted extensive attention due to its flexibility in beam pattern synthesis [5]. However, the introduction and rectification of virtual interference elevate the computational complexity. Algorithms utilizing alternate projection (AP) [6], [7] and related optimization techniques grounded in convex programming (CP) [8], [9] are prevalent and efficient methodologies in the realm of pattern synthesis. These approaches offer flexibility in shaping the desired pattern and can generate magnitude-phase weights or phase-only weights as needed for synthesis purposes. Their advantageous traits include relatively low computational complexity and rapid convergence, rendering them widely embraced and applied in practical application.

For a large-scale array, equipping each element with a dedicated RF channel can be prohibitively costly. To mitigate this expense, sparse array structures [10], [11] or subarray structures [12], [13], [14] are typically employed. Sparse arrays often necessitate the optimization of element placement for specific application scenarios, and reducing antenna elements also results in diminished reception gain.

The associate editor coordinating the review of this manuscript and approving it for publication was Santi C. Pavone.

Subarray structures partition the entire array into multiple regular or irregular subarrays, with each subarray sharing a single RF channel. This approach can significantly reduce the number of required RF channels without reducing the number of antennas. However, the reduction in RF channels introduces challenges in beamforming. Due to the presence of subarrays, grating lobes can easily arise during beam scanning, and the reduced degrees of freedom complicate beam synthesis. In scenarios requiring rapid target search, it becomes necessary to synthesize multiple patterns for the same received signal to expedite the search [15], [16]. Consequently, conventional subarray structures fall short of meeting these demands.

The hybrid beamforming structure [17], commonly used in massive MIMO systems, offers solutions to these challenges. The hybrid beamforming structure facilitates simultaneous multibeam synthesis in the subarray technique. In this structure, a digital phase shifter is added to the end of each antenna, which weights the analog signal input at each antenna before it enters the subarray RF channel. The accuracy of a digital phase shifter is determined by the number of bits, e.g. an 8-bit phase shifter means that the phase of the signal can be controlled with an accuracy of $360/2^8$ degrees, and the amplitude of the signal is controlled by an attenuator. The purpose of this step is to pre-weight the received signals. Without this weighted step, the desired synthesis beams cannot be achieved with the digital weighted after the subarray channels alone, because the number of subarray channels is smaller than the number of antenna units. Subsequently, the subarray signals are subjected to a second step of weighted in the digital beamforming module to adjust the beam shape of the array reception patterns. The weighted at the digital end is fast and can be done multiple times with different weight vectors in a single signal processing cycle to obtain multiple received beam signals simultaneously.

In the second step of weighted, the process is applied to the subarray signals, which are derived from the initial weighted of the array elements. If the weights from the first step are not chosen appropriately, the simultaneous synthesis of multiple beams is inevitably hindered due to the constraints posed by the limited number of subarray channels. Consequently, achieving satisfactory performance for multiple beams requires the identification of an optimal element weighted vectors, along with multiple corresponding subarray weighted vectors.

In light of this scenario, this paper introduces a two-step weighted subarray multiple simultaneous pattern synthesis algorithm. This algorithm is capable of determining element weighted vectors and subarray weighted matrix. By using the Alternate Projection (AP) algorithm, the properties of the Kronecker product [18], and the definition of the Khatri-Rao product [19], the optimal subarray weighted matrix for the element weighted vector can be obtained by solving a 2-norm minimization problem. The AP process is iterated until the synthesis mode meets the requirements, ultimately yielding the required element weighted vector and subarray weighted matrix.

II. PROBLEM STATEMENT

A. PROBLEM MODEL

Consider a large-scale array with N antennas. The antenna elements can be divided into L subarrays, where the lth subarray has N_l elements. It means that the quantity of elements in each subarray can be different. And the total number of antenna elements is N, denoted as $\sum_{l=1}^{L} N_l = N$, where $l = 1, 2, \cdots, L$. The structure diagram is shown in Fig.1.

The response of the array's received signals in various sampling directions can be expressed as

$$\boldsymbol{X} = [\boldsymbol{x}_1, \boldsymbol{x}_2, \cdots, \boldsymbol{x}_N] \tag{1}$$

where $\boldsymbol{x}_n = [x_n(\theta_1, \phi_1), x_n(\theta_2, \phi_2), \cdots, x_n(\theta_K, \phi_K)]^T$. The spatial sampling points can be indicated as (θ_k, ϕ_k),$k = 1, 2, \cdots, K$.

Each antenna is followed by a digitally controlled analog phase shifter. For the received analog signal, the first step of phase shift operation can be performed. The element weighted vector can be represented as

$$\boldsymbol{i} = [i_1, i_2, \cdots, i_N]^T \tag{2}$$

where $\boldsymbol{i}$ is a set of amplitude-phase weighted coefficients and $(\cdot)^T$ is transpose. After weighted the signals of each unit of the same subarray are summed and transmitted to the corresponding RF channel. The subarray transfer matrix with the dimension $N \times L$ can be expressed as

$$\boldsymbol{T} = (t_{n,l})_{N \times L} \tag{3}$$

where $n = 1, 2, \cdots, N$, $l = 1, 2, \cdots, L$. And $t_{n,l} = 1$, if the nth element belongs to the lth subarray. $t_{n,l} = 0$, if the nth element does not belong to the lth subarray. The N elements can be divided into L subarrays through the transformation matrix $\boldsymbol{T}$. The first step, wherein the signal is weighted, segmented based on subarrays, and subsequently directed to the channels, can be symbolized by the following transformation matrix with dimension of $N \times L$

$$\boldsymbol{I} = \mathrm{diag}(\boldsymbol{i})\boldsymbol{T} \tag{4}$$

where diag($\boldsymbol{i}$) represents the diagonal matrix with $\boldsymbol{i}$ as the diagonal elements. At this time, the subarray receiving signal matrix $\boldsymbol{Q}$ is

$$\boldsymbol{Q} = \boldsymbol{X}\boldsymbol{I} \tag{5}$$

Suppose that there are M beams that need to be formed simultaneously, the subarray weighted vectors can be expressed as a matrix $\boldsymbol{W}$ with dimension $L \times M$.

$$\boldsymbol{W} = [\boldsymbol{w}^1, \boldsymbol{w}^2, \cdots, \boldsymbol{w}^M] \tag{6}$$

where $\boldsymbol{w}^m = [w_1^m, w_2^m, \cdots, w_L^m]^T$, $m = 1, 2, \cdots, M$ is the subarray weight of the mth pattern. The ultimate output of multi-beams can be represented by the following matrix $\boldsymbol{F}$

$$\boldsymbol{F} = \boldsymbol{Q}\boldsymbol{W} = [\boldsymbol{F}^1, \boldsymbol{F}^2, \cdots, \boldsymbol{F}^M] \tag{7}$$

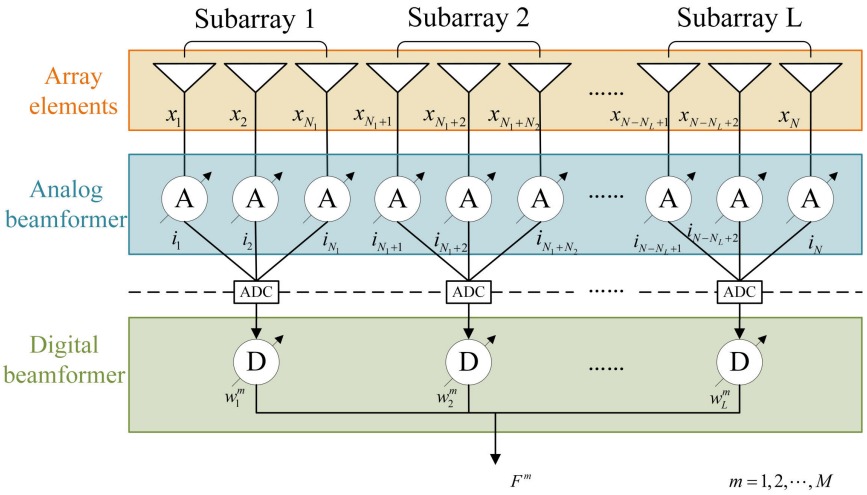

FIGURE 1. Structure diagram of simultaneous multi-pattern hybrid beamforming for subarray phased array.

where $\boldsymbol{F}^m = [\boldsymbol{F}^m(\theta_1, \phi_1), \boldsymbol{F}^m(\theta_2, \phi_2), \cdots, \boldsymbol{F}^m(\theta_K, \phi_K)]^T$ is the mth pattern weighted by $\boldsymbol{w}^m$.

In addition, the target pattern matrix can be expressed as

$$\overline{\boldsymbol{F}} = [\overline{\boldsymbol{F}}^1, \overline{\boldsymbol{F}}^2, \cdots, \overline{\boldsymbol{F}}^M] \tag{8}$$

where $\overline{\boldsymbol{F}}^m = [\overline{\boldsymbol{F}}^m(\theta_1, \phi_1), \overline{\boldsymbol{F}}^m(\theta_2, \phi_2), \cdots, \overline{\boldsymbol{F}}^m(\theta_K, \phi_K)]^T$ is the mth target pattern. Approximating $\boldsymbol{F}$ to $\overline{\boldsymbol{F}}$, the problem of pattern synthesis can be reduced to a matrix minimization problem.

$$\min \quad c\{\boldsymbol{i}, \boldsymbol{W}\} = \left\|\boldsymbol{F} - \overline{\boldsymbol{F}}\right\|_F^2 \tag{9}$$

where $\|\cdot\|_F$ represents the F-norm of a matrix.

B. ALGORITHM DESCRIPTION

According to the problem model, two variables need to be solved. One is the element weighted vector $\boldsymbol{i}$, the other is the subarray weighted matrix $\boldsymbol{W}$. It is very difficult to solve for two variables at the same time. To simplify the problem, solving these two variables separately is a good choice. Firstly, assuming that $\boldsymbol{i}$ is known, solving the expression of $\boldsymbol{W}$. Then using the solved $\boldsymbol{W}$ to calculate the vector $\boldsymbol{i}$.

Defining $\boldsymbol{E} = [\boldsymbol{e}_1, \boldsymbol{e}_2, \cdots, \boldsymbol{e}_M]$ as a M-dimensional identity matrix, where $\boldsymbol{e}_m$ is a unit vector with the mth element equal to 1. Then (9) can be rewritten as

$$\min \quad c\{\boldsymbol{i}, \boldsymbol{W}\} = \left\|\boldsymbol{Q}\boldsymbol{W}\boldsymbol{E}^T - \overline{\boldsymbol{F}}\right\|_F^2 \tag{10}$$

Consider the matrix product $\boldsymbol{Q}\boldsymbol{W}\boldsymbol{E}^T$, where the dimensions of $\boldsymbol{Q}$, $\boldsymbol{W}$, and $\boldsymbol{E}$ are $K \times L$, $L \times M$, and $M \times M$. For simplicity of formula derivation, define $\boldsymbol{w}_l = [w_l^1, w_l^2, \cdots, w_l^M]$ as the lth row of matrix $\boldsymbol{W}$. Then

$$\begin{aligned} \boldsymbol{Q}\boldsymbol{W}\boldsymbol{E}^T &= \left(\sum\nolimits_{l=1}^{L} \boldsymbol{q}_l \boldsymbol{w}_l\right) \boldsymbol{E}^T \\ &= \sum\nolimits_{l=1}^{L} \sum\nolimits_{m=1}^{M} w_l^m \boldsymbol{q}_l \boldsymbol{e}_m^T \end{aligned} \tag{11}$$

Vectorizing (11), by the nature of the Kronecker product, it can be expressed as

$$\begin{aligned} \mathrm{vec}(\boldsymbol{Q}\boldsymbol{W}\boldsymbol{E}^T) &= \mathrm{vec}\left(\sum\nolimits_{l=1}^{L} \sum\nolimits_{m=1}^{M} w_l^m \boldsymbol{q}_l \boldsymbol{e}_m^T\right) \\ &= \sum\nolimits_{l=1}^{L} \sum\nolimits_{m=1}^{M} w_l^m \boldsymbol{e}_m \otimes \boldsymbol{q}_l \\ &= (\boldsymbol{E} \otimes \boldsymbol{Q})\mathrm{vec}(\boldsymbol{W}) \end{aligned} \tag{12}$$

where $\otimes$ is the Kronecker product. The $\mathrm{vec}(\cdot)$ represents the vectorization of a matrix.

Then equation (10) can be written as the 2-norm form

$$\min \quad c\{\boldsymbol{i}, \boldsymbol{W}\} = \left\|(\boldsymbol{E} \otimes \boldsymbol{Q})\boldsymbol{W}_{\mathrm{vec}} - \overline{\boldsymbol{F}}_{\mathrm{vec}}\right\|_2^2 \tag{13}$$

where $\boldsymbol{W}_{\mathrm{vec}} = \mathrm{vec}(\boldsymbol{W})$, $\overline{\boldsymbol{F}}_{\mathrm{vec}} = \mathrm{vec}(\overline{\boldsymbol{F}})$. Based on the property of 2-norm,

$$\begin{aligned} &c\{\boldsymbol{i}, \boldsymbol{W}_{\mathrm{vec}}\} \\ &= [(\boldsymbol{E} \otimes \boldsymbol{Q})\boldsymbol{W}_{\mathrm{vec}} - \overline{\boldsymbol{F}}_{\mathrm{vec}}]^H [(\boldsymbol{E} \otimes \boldsymbol{Q})\boldsymbol{W}_{\mathrm{vec}} - \overline{\boldsymbol{F}}_{\mathrm{vec}}] \\ &= [\boldsymbol{W}_{\mathrm{vec}}^H (\boldsymbol{E} \otimes \boldsymbol{Q})^H - \overline{\boldsymbol{F}}_{\mathrm{vec}}^H][(\boldsymbol{E} \otimes \boldsymbol{Q})\boldsymbol{W}_{\mathrm{vec}} - \overline{\boldsymbol{F}}_{\mathrm{vec}}] \end{aligned} \tag{14}$$

Assuming that $\boldsymbol{i}$ is known. For simplicity of derivation, define $\boldsymbol{B} = \boldsymbol{E} \otimes \boldsymbol{Q}$. Then equation (13) can be written to

$$\begin{aligned} c\{\boldsymbol{W}_{\mathrm{vec}}\} &= [\boldsymbol{W}_{\mathrm{vec}}^H \boldsymbol{B}^H - \overline{\boldsymbol{F}}_{\mathrm{vec}}^H][\boldsymbol{B}\boldsymbol{W}_{\mathrm{vec}} - \overline{\boldsymbol{F}}_{\mathrm{vec}}] \\ &= \boldsymbol{W}_{\mathrm{vec}}^H \boldsymbol{B}^H \boldsymbol{B}\boldsymbol{W}_{\mathrm{vec}} - \boldsymbol{W}_{\mathrm{vec}}^H \boldsymbol{B}^H \overline{\boldsymbol{F}}_{\mathrm{vec}} \\ &\quad - \overline{\boldsymbol{F}}_{\mathrm{vec}}^H \boldsymbol{B}\boldsymbol{W}_{\mathrm{vec}} + \overline{\boldsymbol{F}}_{\mathrm{vec}}^H \overline{\boldsymbol{F}}_{\mathrm{vec}} \end{aligned} \tag{15}$$

Deriving both sides of this equation,

$$\frac{\partial c}{\partial \boldsymbol{W}_{\mathrm{vec}}} = 2\boldsymbol{B}^H \boldsymbol{B}\boldsymbol{W}_{\mathrm{vec}} - 2\boldsymbol{B}^H \overline{\boldsymbol{F}}_{\mathrm{vec}} \tag{16}$$

setting $\partial c / \partial \boldsymbol{W}_{\mathrm{vec}} = 0$, the $\boldsymbol{W}_{\mathrm{vec}}$ can be obtained by

$$\boldsymbol{W}_{\mathrm{vec}} = \left(\boldsymbol{B}^H \boldsymbol{B}\right)^{-1} \boldsymbol{B}^H \overline{\boldsymbol{F}}_{\mathrm{vec}} \tag{17}$$

Obviously, $\boldsymbol{W}$ can be calculated by $\boldsymbol{W}_{\mathrm{vec}}$.

Next using the solved $\boldsymbol{W}$ to calculate the expression of vector $\boldsymbol{i}$. Taking (3), (5), and (7) into (9), the equation can be written as

$$\min \quad c\{\boldsymbol{i}\} = \left\|\boldsymbol{X}\mathrm{diag}(\boldsymbol{i})\boldsymbol{T}\boldsymbol{W} - \overline{\boldsymbol{F}}\right\|_F^2 \tag{18}$$

Defining $\boldsymbol{\Lambda} = \mathrm{diag}(\boldsymbol{i})$, $\boldsymbol{\Omega} = [\boldsymbol{\Omega}_1, \boldsymbol{\Omega}_2, \cdots, \boldsymbol{\Omega}_N] = (\boldsymbol{T}\boldsymbol{W})^T$, equation can be written as

$$\min \quad c\{\boldsymbol{i}\} = \left\|\boldsymbol{X}\boldsymbol{\Lambda}\boldsymbol{\Omega}^T - \overline{\boldsymbol{F}}\right\|_F^2 \tag{19}$$

the matrix product $\boldsymbol{X}\boldsymbol{\Lambda}\boldsymbol{\Omega}^T$ can be written as

$$\begin{aligned}\boldsymbol{X}\boldsymbol{\Lambda}\boldsymbol{\Omega}^T &= \sum_{n=1}^{N} \boldsymbol{x}_n \boldsymbol{\Lambda}_{nn} \boldsymbol{\Omega}_n{}^T \\ &= \sum_{n=1}^{N} \boldsymbol{x}_n \boldsymbol{i}_n \boldsymbol{\Omega}_n{}^T\end{aligned} \tag{20}$$

Based on the definition of Khatri-Rao product ($\odot$), the matrix $\boldsymbol{\Omega}$ and $\boldsymbol{X}$ satisfy that

$$\boldsymbol{\Omega} \odot \boldsymbol{X} = [\boldsymbol{\Omega}_1 \otimes \boldsymbol{x}_1, \boldsymbol{\Omega}_2 \otimes \boldsymbol{x}_2, \cdots, \boldsymbol{\Omega}_N \otimes \boldsymbol{x}_N] \tag{21}$$

Vectorizing (20), it can be expressed as

$$\begin{aligned}vec(\boldsymbol{X}\boldsymbol{\Lambda}\boldsymbol{\Omega}^T) &= \mathrm{vec}(\sum_{n=1}^{N} \boldsymbol{x}_n \boldsymbol{i}_n \boldsymbol{\Omega}_n{}^T) \\ &= [\boldsymbol{\Omega}_1 \otimes \boldsymbol{x}_1, \boldsymbol{\Omega}_2 \otimes \boldsymbol{x}_2, \cdots, \boldsymbol{\Omega}_N \otimes \boldsymbol{x}_N]\boldsymbol{i} \\ &= (\boldsymbol{\Omega} \odot \boldsymbol{X})\boldsymbol{i}\end{aligned} \tag{22}$$

Thus, equation (19) can also be written as the 2-norm form

$$\min \quad c\{\boldsymbol{i}\} = \left\|(\boldsymbol{\Omega} \odot \boldsymbol{X})\boldsymbol{i} - \overline{\boldsymbol{F}}_{vec}\right\|_2^2 \tag{23}$$

For simplicity of derivation, define $\boldsymbol{A} = \boldsymbol{\Omega} \odot \boldsymbol{X}$. Then the $c\{\boldsymbol{i}\}$ can be written to

$$\begin{aligned}c\{\boldsymbol{i}\} &= \left\|\boldsymbol{A}\boldsymbol{i} - \overline{\boldsymbol{F}}_{vec}\right\|_2^2 \\ &= [\boldsymbol{i}^H\boldsymbol{A}^H - \overline{\boldsymbol{F}}_{vec}^H][\boldsymbol{A}\boldsymbol{i} - \overline{\boldsymbol{F}}_{vec}] \\ &= \boldsymbol{i}^H\boldsymbol{A}^H\boldsymbol{A}\boldsymbol{i} - \boldsymbol{i}^H\boldsymbol{A}^H\overline{\boldsymbol{F}}_{vec} \\ &\quad - \overline{\boldsymbol{F}}_{vec}^H\boldsymbol{A}\boldsymbol{i} + \overline{\boldsymbol{F}}_{vec}^H\overline{\boldsymbol{F}}_{vec}\end{aligned} \tag{24}$$

Deriving both sides of this equation,

$$\frac{\partial c}{\partial \boldsymbol{i}_{vec}} = 2\boldsymbol{A}^H\boldsymbol{A}\boldsymbol{i}_{vec} - 2\boldsymbol{A}^H\overline{\boldsymbol{F}}_{vec} \tag{25}$$

setting $\partial c / \partial \boldsymbol{i} = 0$, the $\boldsymbol{i}$ can be obtained by

$$\boldsymbol{i} = \left(\boldsymbol{A}^H\boldsymbol{A}\right)^{-1}\boldsymbol{A}^H\overline{\boldsymbol{F}}_{vec} \tag{26}$$

With the expressions for $\boldsymbol{W}$ and $\boldsymbol{i}$ the alternating projection algorithm can be used to iterate the two-step weights that conform to the desired patterns by giving an initial vector $\boldsymbol{i}$. In each iteration, the calculated synthesis pattern $\boldsymbol{F}^m$ should be projected by upper bound $\boldsymbol{E}_{up}$ and lower bound $\boldsymbol{E}_{low}$ of the desired patterns.

$\overline{F}^m(\theta_k, \phi_k)$

$$= \begin{cases} E_{up}^m(\theta_k, \phi_k)\dfrac{F^m(\theta_k, \phi_k)}{|F^m(\theta_k, \phi_k)|}, \\ \quad \left|F^m(\theta_k, \phi_k)\right| > E_{up}^m(\theta_k, \phi_k) \\ F^m(\theta_k, \phi_k), \\ \quad E_{\mathrm{low}}^m(\theta_k, \phi_k) \le \left|F^m(\theta_k, \phi_k)\right| \le E_{up}^m(\theta_k, \phi_k) \\ E_{low}^m(\theta_k, \phi_k)\dfrac{F^m(\theta_k, \phi_k)}{|F^m(\theta_k, \phi_k)|}, \\ \quad \left|F^m(\theta_k, \phi_k)\right| < E_{\mathrm{low}}^m(\theta_k, \phi_k) \end{cases} \tag{27}$$

where $\boldsymbol{E}_{up} = [\boldsymbol{E}_{up}^1, \boldsymbol{E}_{up}^2, \cdots, \boldsymbol{E}_{up}^M]$ and $\boldsymbol{E}_{low} = [\boldsymbol{E}_{low}^1, \boldsymbol{E}_{low}^2, \cdots, \boldsymbol{E}_{low}^M]$. The mth($m = 1, 2, \cdots, M$) pattern's upper bound and lower bound are

$$\begin{aligned}\boldsymbol{E}_{up}^m &= [E_{up}^m(\theta_1, \phi_1), E_{up}^m(\theta_2, \phi_2), \cdots, E_{up}^m(\theta_K, \phi_K)]^T, \\ \boldsymbol{E}_{low}^m &= [E_{low}^m(\theta_1, \phi_1), E_{low}^m(\theta_2, \phi_2), \cdots, E_{low}^m(\theta_K, \phi_K)]^T.\end{aligned}$$

After projecting, the pattern $\overline{\boldsymbol{F}}^m$ can be used as a target pattern for the next iterate. The algorithm steps can be summarized as **Algorithm 1**. Then the desired patterns can be obtained.

Algorithm 1 Simultaneous Multiple Pattern Synthesis

1: Initialize the $\boldsymbol{i}^{(n)}$, $\boldsymbol{W}^{(n)}$, $\boldsymbol{E}_{up}$ and $\boldsymbol{E}_{low}$ ($n = 0$).
2: Substitute $\boldsymbol{i}^{(n)}$ and $\boldsymbol{W}^{(n)}$ into (7) to calculate $\boldsymbol{F}^{(n)}$.
3: Compare the synthesis pattern $\boldsymbol{F}^{(n)}$ with $\boldsymbol{E}_{up}$ and $\boldsymbol{E}_{low}$. Using (27), the target pattern $\overline{\boldsymbol{F}}^{(n)}$ can be obtained.
4: Substitute $\boldsymbol{i}^{(n)}$ and $\overline{\boldsymbol{F}}^{(n)}$ into (17) to calculate $\boldsymbol{W}^{(n+1)}$.
5: Substitute $\boldsymbol{W}^{(n+1)}$ into (26) to calculate $\boldsymbol{i}^{(n+1)}$.
6: Substitute $\boldsymbol{i}^{(n+1)}$ and $\boldsymbol{W}^{(n+1)}$ into (7) to calculate $\boldsymbol{F}^{(n+1)}$.
7: If $\boldsymbol{F}^{(n+1)}$ meets the requirements, the iteration is over. If not, let $n = n + 1$ and repeat the steps 3-7.

To speed up the convergence, an inner iteration is added to algorithm 1. Keeping the target pattern $\overline{\boldsymbol{F}}^{(n)}$ constant, replace the $\boldsymbol{i}^{(n)}$ in step 4 with $\boldsymbol{i}^{(n,j)}$ calculated in step 5 and repeat the steps, until the $\boldsymbol{i}^{(n+1,j+1)}$ and $\boldsymbol{i}^{(n,j)}$ are satisfied that

$$\varepsilon = \frac{\left\|\boldsymbol{i}^{(n+1,j+1)} - \boldsymbol{i}^{(n,j)}\right\|}{\left\|\boldsymbol{i}^{(n,j)}\right\|} < \varepsilon_0 \tag{28}$$

where $j = 0, 1, \cdots, (J-1)$ is the order of the inner iteration, ε_0 is a preset error value. The improved algorithm steps can be summarized as **Algorithm 2**. Meanwhile, Table 1 lists the complexity of each step of Algorithm 1 and Algorithm 2.

III. SIMULATION AND MEASUREMENT

To verify the effectiveness of the proposed algorithm, a subarray multi-beam synthesis simulation is provided in this section. The antenna element is a vivaldi antenna and the design parameters are shown in Fig.2 and Table 2. The antenna is a broadband antenna, and the operating frequency of the antenna is set to 10 GHz for this simulation experiment. Consider the planar array with 336 elements in Fig.3(a), which are arranged in triangular raster form. The distances of

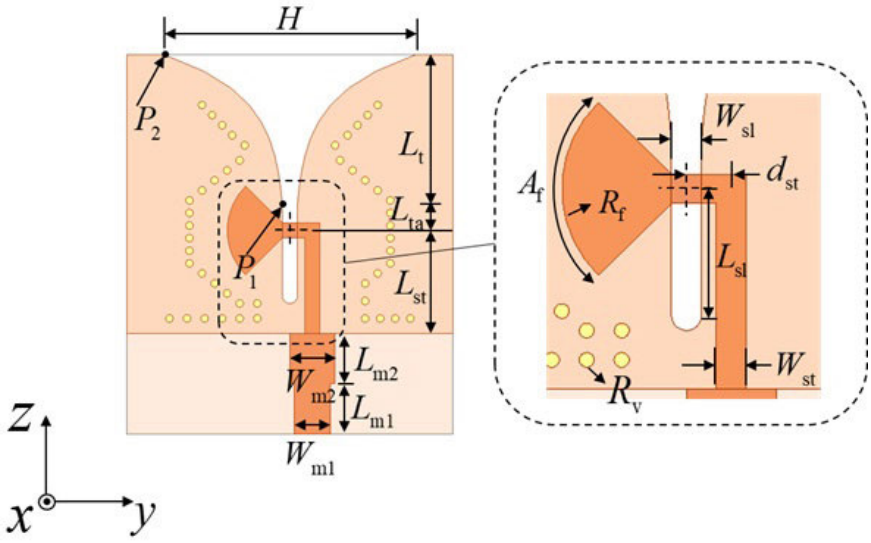

FIGURE 2. The parameters of the vivaldi antenna.

Algorithm 2 Improved Algorithm of 1

1: Initialize the ε_0, $\boldsymbol{i}^{(n)}$, $\boldsymbol{W}^{(n)}$, $\boldsymbol{E}_{up}$ and $\boldsymbol{E}_{low}$ $(n = 0)$.
2: Substitute $\boldsymbol{i}^{(n)}$ and $\boldsymbol{W}^{(n)}$ into (7) to calculate $\boldsymbol{F}^{(n)}$.
3: Compare the synthesis pattern $\boldsymbol{F}^{(n)}$ with $\boldsymbol{E}_{up}$ and $\boldsymbol{E}_{low}$. Using (27), the target pattern $\overline{\boldsymbol{F}}^{(n)}$ can be obtained.
4: Let $\boldsymbol{i}^{(n,j)} = \boldsymbol{i}^{(n)}$ $(j = 0)$.
5: Substitute $\boldsymbol{i}^{(n,j)}$ and $\overline{\boldsymbol{F}}^{(n)}$ into (17) to calculate $\boldsymbol{W}^{(n+1,j+1)}$.
6: Substitute $\boldsymbol{W}^{(n+1,j+1)}$ into (26) to calculate $\boldsymbol{i}^{(n+1,j+1)}$.
7: If $\boldsymbol{i}^{(n,j)}$ and $\boldsymbol{i}^{(n+1,j+1)}$ meet the requirements of (28), the iteration is over and let $\boldsymbol{i}^{(n+1)} = \boldsymbol{i}^{(n+1,j+1)}$, $\boldsymbol{W}^{(n+1)} = \boldsymbol{W}^{(n+1,j+1)}$. If not, let $\boldsymbol{i}^{(n,j+1)} = \boldsymbol{i}^{(n+1,j+1)}$, $j = j + 1$ and repeat the steps 5-6.
8: Substitute $\boldsymbol{i}^{(n+1)}$ and $\boldsymbol{W}^{(n+1)}$ into (7) to calculate $\boldsymbol{F}^{(n+1)}$.
9: If $\boldsymbol{F}^{(n+1)}$ meets the requirements, the iteration is over. If not, let $n = n + 1$ and repeat the steps 3-8.

TABLE 1. Complexity of algorithm 1 and algorithm 2.

Step	Algorithm 1 complexity	Algorithm 2 complexity
1	$O(max(KM, N, LM))$	$O(max(KM, N, LM))$
2	$O(KN^2)$	$O(KN^2)$
3	$O(KM)$	$O(KM)$
4	$O(KM^3L^2)$	$O(N)$
5	$O(max(KM, N)N^2)$	$O(KM^3L^2)$
6	$O(KN^2)$	$O(max(KM, N)N^2)$
7	$O(KM)$	$O(N)$
8	/	$O(KN^2)$
9	/	$O(KM)$

adjacent elements along x-axis and y-axis are $d_x = 0.508\lambda$ and $d_y = 0.587\lambda$. The array is divided into 84 subarrays, each subarray has 4 elements. For easy observation, the elements of the same subarray are circled by rectangular boxes. The full array is modeled in "Ansys Electronics Desktop 2022 R2"

TABLE 2. The parameter values of vivaldi antenna.

Parameter	Value (mm)	Parameter	Value (mm)	Parameter	Value (mm)
H	10	W_{sl}	0.6	W_{st}	0.6
L_t	6	d_{st}	0.9	W_{m1}	1.45
L_{ta}	1	R_f	2.5	W_{m2}	1.8
L_{st}	4.1	L_{m1}	2	R_V	0.15
L_{sl}	2.6	L_{m2}	2	A_f	$\pi/2$(rad)

TABLE 3. Maximum directivity of the synthesized beams for each method.

No.	Pattern directivity of proposed method (dB)	Pattern directivity of AP method (dB)	Pattern directivity of GA method (dB)
1	16.09	17.39	15.96
2	16.50	17.61	16.22
3	16.57	17.05	16.28
4	16.21	17.38	16.07
5	16.05	17.48	16.23
6	15.98	17.29	16.27

for full-wave simulation, and the active element pattern of each element is exported for pattern synthesis simulation in "MATLAB R2022b".

In a guide head radar target search scenario, the beamforming requirements for simultaneous multi-beams consist of six segments forming a conical beam. Therefore, the 6 different patterns of the cone beam are used as the desired patterns. The coverage regions of them on uv-plane are shown in Fig.3(b), where $u = \sin(\theta)\cos(\phi)$, $v = \sin(\theta)\sin(\phi)$. The tilt angle of the cone is $\theta = 35°$ and the width of the cone is 10°. The rotation angles ϕ of the 6 patterns are $(-30°, 30°)$, $(30°, 90°)$, $(90°, 150°)$, $(150°, 210°)$, $(210°, 270°)$ and $(270°, 330°)$, which defined as number 1-6.

According to the 6 coverage areas in Fig.3(b), the footprints of desired patterns are shown in Fig.4. Footprints

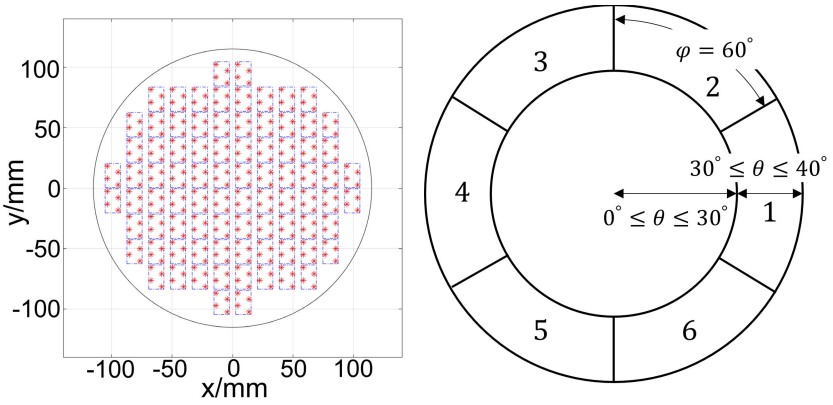

(a) Array model and subarrays with rectangular boxes. (b) The coverage regions of 6 different areas.

FIGURE 3. Planar array model and pattern coverage regions.

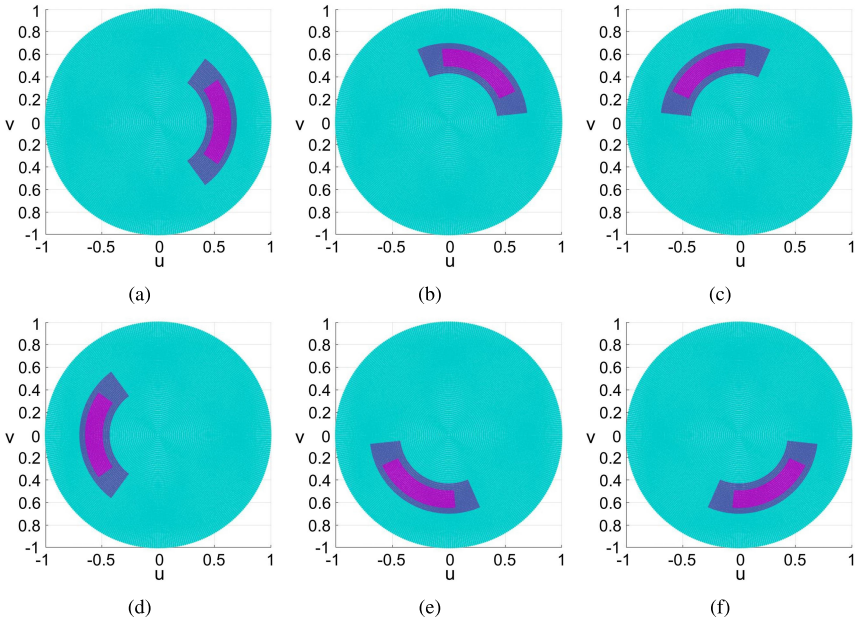

FIGURE 4. The footprints of desired patterns.

are the target of beam synthesis and comprises the main lobe area, transition area, and side lobe area. In the figures of Fig.4, the purple area in each footprint illustrates the main lobe region of the corresponding pattern. Dark purple indicates the transition region, and cyan represents the side lobe region. Constrain the minimum amplitude of the pattern's main lobe area to −3dB, set the highest side lobe level to -20dB, and leave the transition area unconstrained. With the proposed method, the element weighted vector and subarray weighted matrix can be calculated. And the simulated results of desired patterns are shown in Fig.5. We can observe that the 6 beam patterns obtained through simulation consistently adhere to their beam footprints. Fig.6 shows the normalized gain contour plot of the direction map obtained from the simulation, where the green region is the main lobe region of the target patterns, and the red line is the −3dB contour of the patterns. The shape of their main lobes meets the performance requirements, and the maximum ripple in the main lobe does not exceed 1.5dB. Their highest side lobe levels are around -20dB.

In the following discussion, we will explore the influence of the improved algorithm on convergence speed. Fig.7(a) shows the number of internal iterations corresponding to each external iteration, highlighting the phenomenon that when the number of external iterations is low, the number of internal iterations is high. At the very beginning of the external iterations, the array element weight vectors require several internal iterations to stabilize. As the external iterations progress, the array element weight vector parameters gradually stabilize, and eventually the number of internal

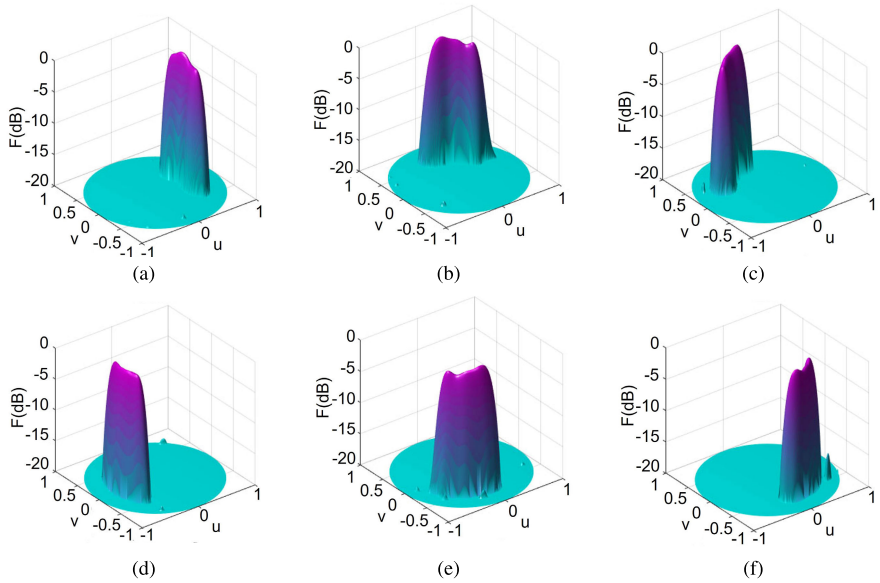

FIGURE 5. The simulation results of desired patterns.

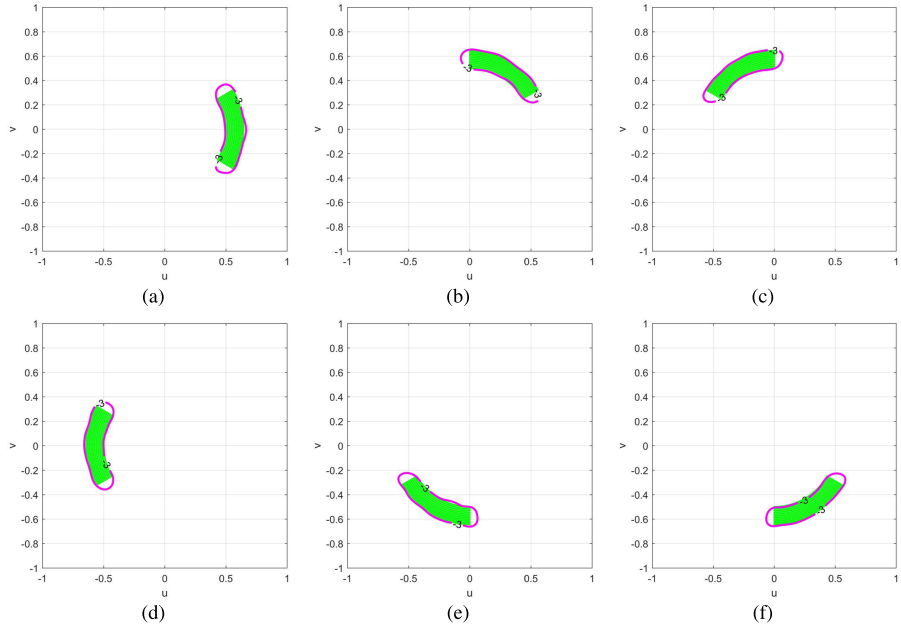

FIGURE 6. The contour map of simulated patterns.

iterations is reduced to one. Fig.7(b) shows the internal iteration error, demonstrating the difference between the array element weight vectors at the beginning and end of the internal iterations in each external iteration.

Fig.8 illustrates the comparison of the synthesized patterns generated by the proposed algorithm with the synthesized patterns generated by the full-array AP method and the genetic algorithm in the two-step weighted structure. Without loss of generality, the comparison is made using the 2D slices of beam #3 and #5 at $\theta = 35°$. From Fig.8, it is evident that the maximum directivity of the simultaneous multibeam patterns within the two-step weighted structure experiences a reduction of approximately 1.2 dB in comparison to the full array. Since the channel degrees of freedom of the two-step weighted structure are less than those of the full array, the main flap ripples and directionality performances are predictably worse than in the full array. Fortunately, this discrepancy is minor. Although there isn't a substantial variance in directivity when compared to the global optimal solution discovered by the genetic algorithm, there is a slight increase in the magnitude of main flap ripples. However, the computational complexity of the proposed method is

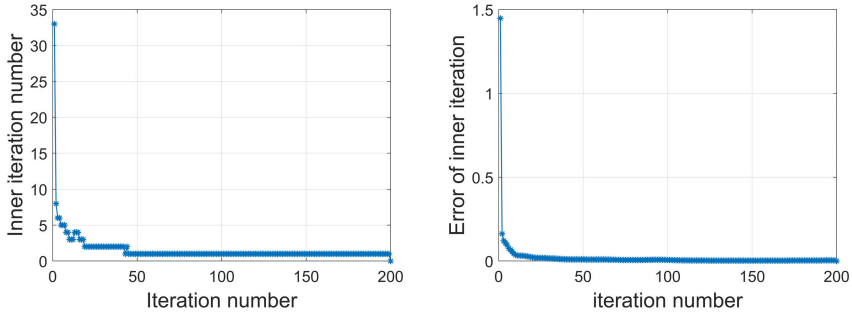

(a) Relationship between inner iteration number and iteration number.

(b) Relationship between error of inner iteration and iteration number.

FIGURE 7. Impact of algorithm 2 on iteration efficiency.

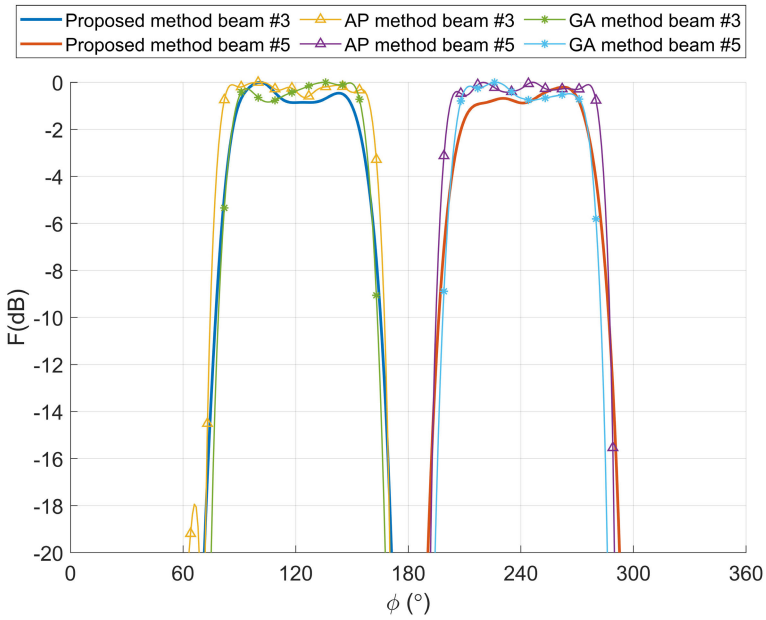

FIGURE 8. The 2D slice figures of beams #3 and #5 under 3 methods when $\theta = 35°$.

much less compared to the genetic algorithm. The maximum directivity of the synthesized beams for each method is shown in Table 3.

The element weighted vector $\boldsymbol{i}$ and the subarray weighted matrix $\boldsymbol{W}$ calculated by the simulated are tested on the guide head radar prototype shown in Fig.9(a). The microwave anechoic chamber measurement environment is shown in Fig.9(b). The steps for array testing in a microwave anechoic chamber are as follows: (1) Set up the test link in the microwave anechoic chamber, and set the prototype to receiving mode after system calibration. (2) The waveguide probe outputs energy on a large plane 3 wavelengths away from the antenna array at angular intervals preset by the test system. (3) The near-field signal received by the prototype antenna is processed and calculated to calculate a three-dimensional receiving pattern based on the near-field test. (4) The near-field three-dimensional pattern is input into the near/far field conversion program of the test system, and the far-field receiving beam pattern can be output.

The six 3D beam patterns measured in a microwave anechoic chamber are illustrated in Fig.10. To enhance visibility of the beam positions, the figures are presented from a top view perspective. Additionally, the original simulation's uv coordinate labels were replaced with azimuth and elevation coordinate labels in the testing environment.

As depicted in Fig.10, the test results of the six beams align closely with the simulation results. Nonetheless, there is a slight degradation observed in the main lobe shape and side lobe levels. The Fig.11 is the contour map of the measured patterns, where the green area in each figure represents the main lobe shape of the desired pattern. The red and blue curves are the 3dB and 10dB contour curves of each measured pattern respectively. It is evident that beams #2 and #5 exhibit a degradation in the main lobe shape. The Fig.12 shows the

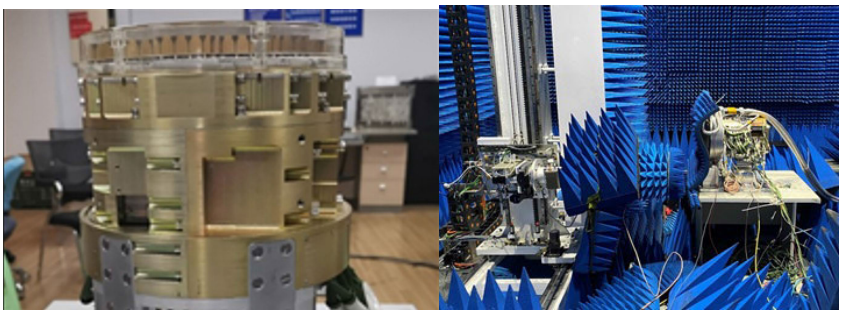

(a) The photo of the guide head radar prototype. (b) Microwave anechoic chamber measurement environment.

FIGURE 9. Prototype and measurement environment.

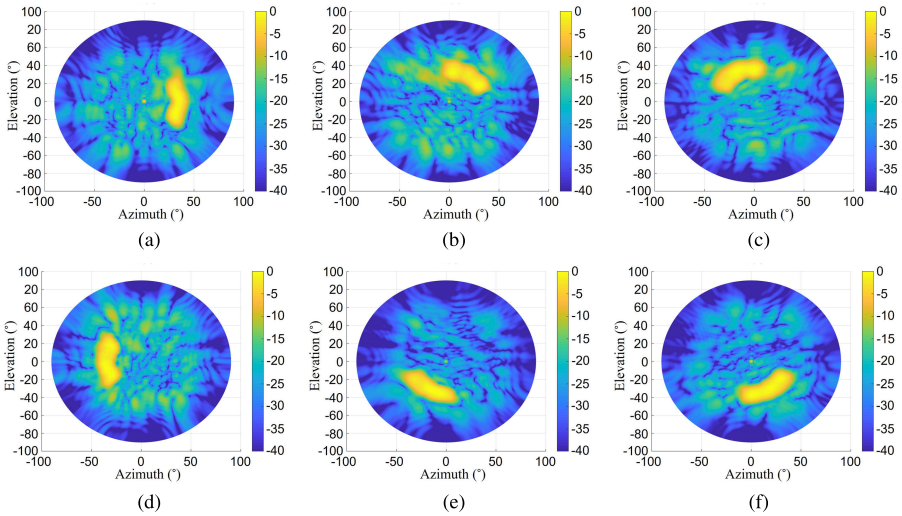

FIGURE 10. The top view of the measured patterns.

2D slice figures of 6 beams respect to ϕ when $\theta = 35°$, where lines in six distinct colors dark blue, red, yellow, purple, green, and light blue are employed to denote beams 1-6. Solid lines represent simulated beams, while dashed lines with '*' symbols represent measured beams. Fig.12 reveals that, in comparison to the simulation results, although there is a deterioration in the main lobe shape, the ripple remains within 3dB. However, the highest level of the side lobe has degraded from approximately -20dB in the simulation results to around -16dB. Additional parameter comparisons between simulated and measured patterns are detailed in Table 4.

So far, the effectiveness of the proposed algorithm is proved by simulation. The array element weighted vector and subarray weighted matrix obtained from the simulation are loaded into the 336-unit guide head radar prototype for receiving pattern test, and the test results are consistent with the simulation results, which proves the feasibility of the algorithm.

It is worth noting that typically, 50% of the cost of an all-channel digital receiver array is concentrated in the RF channels, 20% in the antennas, 20% in the signal processing modules, and 10% in other hardware costs. Utilizing the subarray technique (where 4 units form a subarray as exemplified in this paper), the array's channel and signal processing module costs are reduced to 1/4 of the total cost of an all-channel array. The additional cost incurred by integrating digital phase shifters per antenna is significantly less than the savings achieved, which amounts to 3/4 of the total cost of an all-channel array. Furthermore, as the number of channels is reduced, there is a proportional decrease in the number of boards required in the signal processing module, leading to potential reductions in both weight and size of the

TABLE 4. Parameters of simulated and measured patterns.

No.	Mainlobe ripple of simulated pattern (dB)	Mainlobe ripple of measured pattern (dB)	Sidelobe level of simulated pattern (dB)	Sidelobe level of measured pattern (dB)
1	1.0	0.8	-18.5	-13.6
2	1.5	2.5	-19.2	-9.9
3	1.2	0.9	-18.8	-11.0
4	0.2	1.8	-19.1	-9.4
5	0.8	2.7	-18.6	-13.8
6	0.9	0.8	-16.2	-14.5

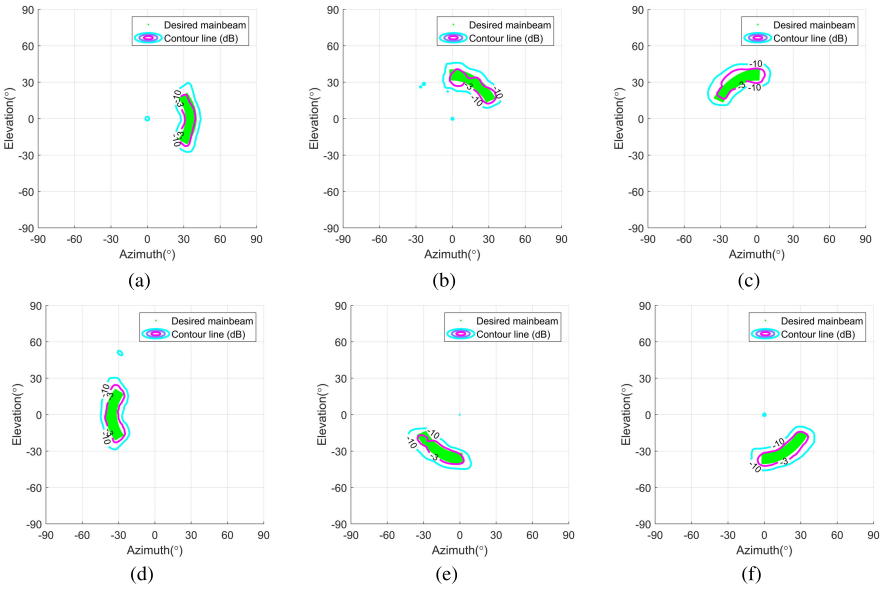

FIGURE 11. The contour map of measured patterns.

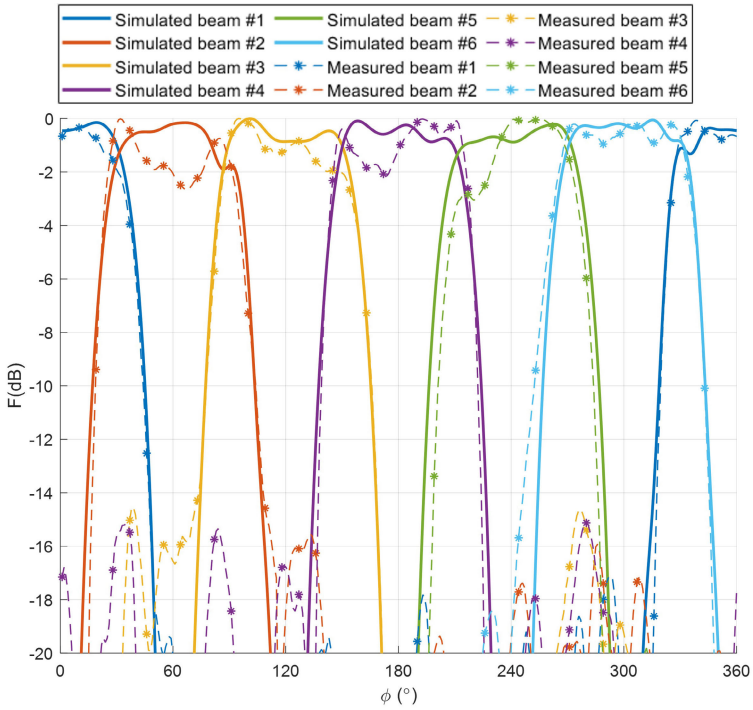

FIGURE 12. The 2D slice figures of 6 beams when $\theta = 35°$.

prototype. Consequently, adopting the architecture proposed in this paper proves to be economically advantageous.

IV. CONCLUSION

The simultaneous multiple pattern synthesis algorithm for subarray is proposed in this paper. Using this method, the element weighted vector and subarray weighted matrix can be obtained. Through simulation and measurement, the effectiveness of the method is proved. Employing subarray technology can significantly reduce the number of required radio frequency channels, resulting in cost savings for the entire system. Ensuring beam performance of received signals is achievable through the implementation of a two-step weighted hybrid structure. This approach finds utility in applications like guide head radar target detection, enhancing efficiency by saving time during target search through the use of simultaneous multi-beam algorithms.

ACKNOWLEDGMENT

The authors would like to thank the Array Antenna and Array Signal Processing Laboratory of Nanjing University of Science and Technology for their assistance.

REFERENCES

[1] B. K. Lau and Y. H. Leung, "A Dolph-Chebyshev approach to the synthesis of array patterns for uniform circular arrays," in *Proc. IEEE Int. Symp. Circuits Systems. Emerg. Technol. 21st Century.*, vol. 1, Geneva, Switzerland, 2000, pp. 124–127, doi: 10.1109/ISCAS.2000.857042.

[2] J.-Y. Li, Y.-X. Qi, and S.-G. Zhou, "Shaped beam synthesis based on superposition principle and Taylor method," *IEEE Trans. Antennas Propag.*, vol. 65, no. 11, pp. 6157–6160, Nov. 2017, doi: 10.1109/TAP.2017.2754468.

[3] M. E. Yigit and T. Gunel, "Pattern synthesis of linear antenna array via a new hybrid Taguchi–genetic–particle swarm optimization algorithm," in *Proc. 18th Medit. Microw. Symp. (MMS)*, Istanbul, Turkey, Oct. 2018, pp. 17–21, doi: 10.1109/MMS.2018.8611954.

[4] Y. Jiang, S. Zhang, Q. Guo, and X. Luan, "A hybrid strategy based on weighting density and genetic algorithm for the synthesis of uniformly weighted concentric ring arrays," *IEEE Antennas Wireless Propag. Lett.*, vol. 16, pp. 186–189, 2017, doi: 10.1109/LAWP.2016.2567785.

[5] X. Ai and L. Gan, "Precise array response control for beampattern synthesis with minimum pattern distortion," *Signal Process.*, vol. 192, Mar. 2022, Art. no. 108395, doi: 10.1016/j.sigpro.2021.108395.

[6] J. L. A. Quijano and G. Vecchi, "Alternating adaptive projections in antenna synthesis," *IEEE Trans. Antennas Propag.*, vol. 58, no. 3, pp. 727–737, Mar. 2010, doi: 10.1109/TAP.2009.2039307.

[7] Y. Han, C. Wan, W. Sheng, B. Tian, and H. Yang, "Array synthesis using weighted alternating projection and proximal splitting," *IEEE Antennas Wireless Propag. Lett.*, vol. 14, pp. 1006–1009, 2015, doi: 10.1109/LAWP.2015.2389804.

[8] G. M. Battaglia, A. F. Morabito, G. Sorbello, and T. Isernia, "Mask-constrained power synthesis of large and arbitrary arraysas a few-samples global optimization," *Prog. Electromagn. Res. C*, vol. 98, pp. 69–81, 2020, doi: 10.2528/pierc19082904.

[9] G. M. Battaglia, G. G. Bellizzi, A. F. Morabito, G. Sorbello, and T. Isernia, "A general effective approach to the synthesis of shaped beams for arbitrary fixed-geometry arrays," *J. Electromagn. Waves Appl.*, vol. 33, no. 18, pp. 2404–2422, Dec. 2019, doi: 10.1080/09205071.2019.1683472.

[10] I. Aboumahmoud, A. Muqaibel, M. Alhassoun, and S. Alawsh, "A review of sparse sensor arrays for two-dimensional direction-of-arrival estimation," *IEEE Access*, vol. 9, pp. 92999–93017, 2021, doi: 10.1109/ACCESS.2021.3092529.

[11] L. Zhang, W. Cui, B. Ba, C. Jian, and H. Li, "A DOA estimation method for sparse array based on DFT spectrum of received signals," *IEEE Access*, vol. 10, pp. 95849–95858, 2022, doi: 10.1109/access.2022.3205343.

[12] Y. Li, Y. Gong, and S. Xiao, "Synthesis of modular subarrayed phased-array with shaped-beams by means of sequential convex optimization," *IEEE Antennas Wireless Propag. Lett.*, vol. 21, pp. 1168–1172, 2022, doi: 10.1109/LAWP.2022.3160733.

[13] Q. Zhao, P. Gu, D. Ding, and R. Chen, "Pattern synthesis of planar phased arrays via subarray division with user freedom," in *Proc. Cross Strait Radio Sci. Wireless Technol. Conf. (CSRSWTC)*, Fuzhou, China, Dec. 2020, pp. 1–3, doi: 10.1109/CSRSWTC50769.2020.9372506.

[14] Q. An, C. Yeh, Y. Lu, Y. He, and J. Yang, "A convex optimization based multistage wideband pattern accurate synthesis method for overlapping subarrays," *Signal Process.*, vol. 213, Dec. 2023, Art. no. 109197, doi: 10.1016/j.sigpro.2023.109197.

[15] Y. Aslan, J. Puskely, A. Roederer, and A. Yarovoy, "Multiple beam synthesis of passively cooled 5G planar arrays using convex optimization," *IEEE Trans. Antennas Propag.*, vol. 68, no. 5, pp. 3557–3566, May 2020, doi: 10.1109/TAP.2019.2955885.

[16] H. Zeng, Z.-H. Xu, G.-Q. Yang, and S.-P. Xiao, "Multiple simultaneous receive beam synthesis of overlapped subarray structure via alternative sequential convex programming," *IEEE Antennas Wireless Propag. Lett.*, vol. 20, pp. 1190–1194, 2021, doi: 10.1109/LAWP.2021.3075058.

[17] S. Han, Z. Xu, and S. Wang, "Reference signals design for hybrid analog and digital beamforming," *IEEE Commun. Lett.*, vol. 18, no. 7, pp. 1191–1193, Jul. 2014, doi: 10.1109/LCOMM.2014.2317747.

[18] X. Wang, J. Benesty, J. Chen, G. Huang, and I. Cohen, "Beamforming with cube microphone arrays via Kronecker product decompositions," *IEEE/ACM Trans. Audio, Speech, Lang., Process.*, vol. 29, pp. 1774–1784, 2021, doi: 10.1109/TASLP.2021.3079816.

[19] J. Konishi, H. Yamada, and Y. Yamaguchi, "On optimum element arrangements of MIMO radar based on the Khatri-rao product virtual array," in *Proc. Int. Symp. Antennas Propag. (ISAP)*, Busan, South Korea, Oct. 2018, pp. 1–2.

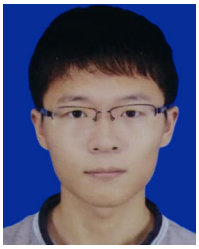

ZHONGTIAN JING was born in Zhenjiang, Jiangsu, China, in 1995. He received the B.S. degree from Nanjing University of Science and Technology, Nanjing, China, in 2018, where he is currently pursuing the Ph.D. degree with the School of Electronic and Optical Engineering.

His current research interests include phased array, conformal array, beam synthesis, and array mutual coupling estimation.

YUBING HAN (Member, IEEE) was born in 1971. He received the Ph.D. degree in signal and information processing from Southeast University, China, in 2006.

From 2007 to 2009, he was a Postdoctoral Researcher with the Department of Electronic Engineering, Nanjing University of Science and Technology (NJUST), Nanjing, China. Since 2006, he has been a Faculty Member with the School of Electronic and Optical Engineering, NJUST, where he is currently a Professor. From 2009 to 2010, he was a Visiting Scholar with the Department of Electrical and Computer Engineering, Brigham Young University, Provo, UT, USA. His current research interests include sensor signal processing, radar signal processing, wireless communications, and digital image processing.

YUCHEN FENG was born in Xuzhou, Jiangsu, China, in 2000. She received the Bachelor of Engineering degree in electronics and communication from Nanjing University of Science and Technology, Nanjing, China, in 2021, where she is currently pursuing the master's degree with the School of Electronic and Optical Engineering.

Her current research interests include array beamforming, array beamshaping, and phased array.

LEI XIAO was born in 1993. He received the B.S. degree from the School of Electronic and Optical Engineering, Nanjing University of Science and Technology (NJUST), Nanjing, China, in 2015. He is currently pursuing the Ph.D. degree in information and communication engineering with NJUST.

His current research interests include low-cost digital phased array, radar signal processing, and compressed sensing.